New insights on the HCl abundance in the interstellar medium

M. Lanza, Y. Kalugina, L. Wiesenfeld, A. Faure, F. Lique

Monthly Notices
of the
ROYAL ASTRONOMICAL SOCIETY

MNRAS **443,** 3351–3358 (2014) doi:10.1093/mnras/stu1371

New insights on the HCl abundance in the interstellar medium

M. Lanza,[1⋆] Y. Kalugina,[1,2] L. Wiesenfeld,[3] A. Faure[3] and F. Lique[1⋆]

[1]*LOMC - UMR 6294, CNRS-Université du Havre, 25 rue Philippe Lebon, BP 540, F-76058 Le Havre, France*
[2]*Department of Optics and Spectroscopy, Tomsk State University, 36 Lenin av., Tomsk 634050, Russia*
[3]*UJF-Grenoble 1/CNRS, Institut de Planétologie et d'Astrophysique de Grenoble (IPAG) UMR 5274, Grenoble F-38041, France*

Accepted 2014 July 6. Received 2014 July 4; in original form 2014 April 18

ABSTRACT

HCl is supposed to be one of the main chlorine carriers in the interstellar medium (ISM). Then, accurate knowledge of chlorine chemistry requires accurate estimating the HCl abundance in molecular clouds which in turn requires the calculation of collisional excitation rate coefficients for the HCl molecule due to collisions with the most abundant collisional partner in the ISM. In this paper, we report theoretical calculations of the HCl–H_2 rotationally inelastic rate coefficients. Using a recently developed potential energy surface, we have computed rate coefficients between the first 11 rotational levels of HCl for temperatures ranging from 5 to 300 K. These new HCl–H_2 rate coefficients were compared to the available HCl–He rate coefficients currently used for astrophysical modelling. As one would expect, significant differences were found between new HCl–H_2 and previous HCl–He rate coefficients. As a first application, we simulate the excitation of HCl in typical star-forming regions and in protostellar shocks. Electron-impact excitation is also included. It is found that the new H_2 rate coefficients significantly increase the simulated line intensities. As a consequence, HCl abundance derived from the observations will be significantly reduced by the use of the present rate coefficients, confirming that HCl may not be the main chlorine carrier in the ISM.

Key words: molecular data – molecular processes – ISM: abundances.

1 INTRODUCTION

Chlorine has two stable isotopes, ^{35}Cl and ^{37}Cl, and a relatively low solar abundance of 3.2×10^{-7} relative to atomic hydrogen (Asplund et al. 2009). In the interstellar medium (ISM), chlorine has been mostly observed in molecular hydrides like HCl (Blake, Keene & Phillips 1985), H_2Cl^+ (Luca et al. 2012) or HCl^+ (Lis et al. 2010; Neufeld et al. 2012). Some metal halides with chlorine, NaCl, AlCl and KCl, have also been detected towards the late-type carbon star IRC+10216 (Cernicharo & Guelin 1987). The simplest chlorine hydride, HCl, is then expected to be an important reservoir of chlorine, especially in the dense regions of the ISM where hydrogen is predominantly molecular (Neufeld & Wolfire 2009).

In diffuse interstellar clouds, chlorine chemistry is relatively simple. Corresponding reactive rate constants can be found in Wakelam et al. (2012). Chlorine atom has a first ionization potential (12.97 eV) smaller than the one of atomic hydrogen (13.6 eV; Lide 2008). Thus, chlorine is not shielded from the interstellar radiation field (ISRF) by hydrogen and this explains why Cl^+ is the dominant form of atomic chlorine in diffuse clouds. Cl^+ can still react exothermically with H_2 (Smith & Adams 1981) since the dissociative energy of HCl^+ (4.64 eV) is larger than that of molecular hydrogen (4.48 eV; Lide 2008). This occurs in regions where H_2 is abundant:

$$Cl^+ + H_2 \rightarrow HCl^+ + H.$$

Then, HCl^+, if not destroyed by a dissociative recombination (Novotný et al. 2013), can in turn react with H_2 to form H_2Cl^+:

$$HCl^+ + H_2 \rightarrow H_2Cl^+ + H.$$

Dissociative recombination of H_2Cl^+ then leads to the formation of HCl or Cl such as

$$H_2Cl^+ + e^- \rightarrow HCl + H \text{ or } Cl + 2H.$$

Note that the product branching ratios for the dissociative recombination of H_2Cl^+ is uncertain but recent measurements on the deuterated isotopologue D_2Cl^+ suggest that the DCl + D channel has a branching ratio of at least 10 per cent (Novotný et al. 2012) and that the dominant channel is the three-body breaking.

In the diffuse ISM, HCl was first (tentatively) identified by Federman et al. (1995) towards ζ Ophiuchi *via* ultraviolet absorption lines with the *Hubble Space Telescope*. More recently, HCl was detected in diffuse clouds towards the star-forming region W31C using the heterodyne instrument for the far-infrared (HIFI) on board the *Herschel Space Observatory* (Monje et al. 2013). The $j = 1-0$ lines of the two stable HCl isotopologues, $H^{35}Cl$ and $H^{37}Cl$, were

⋆ E-mail: mathieu.lanza@univ-lehavre.fr (ML); francois.lique@univ-lehavre.fr (FL)

observed in absorption. The analysis of Monje et al. (2013) suggests that HCl accounts for ~ 0.6 per cent of the total gas-phase chlorine, which exceeds by a factor of about 6 the theoretical predictions.

In dense molecular clouds, chlorine chemistry is more complex (Neufeld & Wolfire 2009). In particular, the abundance of HCl is expected to vary with the depth in the molecular clouds. The cloud surface is exposed to the ISRF and chlorine is mostly in the Cl^+ form, as in diffuse clouds. At larger depth below the cloud surface (corresponding to a visual extinction $A_V \gtrsim 1$), reaction with H_2 is the dominant destruction process for Cl^+, as mentioned above. Electrons tend to dissociate HCl^+ before it can form H_2Cl^+ so that neutral Cl is the dominant form of chlorine. In the deep cloud interiors ($A_V \gtrsim 4$), electron abundance is very low and reactive collisions between Cl and H_3^+ lead either to formation of HCl^+, which then reacts with H_2 to form H_2Cl^+, or directly to the formation of H_2Cl^+. As there are not enough electrons to dissociate the molecular ions, H_2Cl^+ could transfer one of its proton to neutral species such as CO, leading to the formation of HCl. At these large depths into the cloud, HCl is shielded from the ISRF and the HCl destruction rate is small. HCl is thus expected to be the most abundant chlorine-bearing molecule and it is predicted to account for about 10–30 per cent of the gas-phase chlorine abundance, the remaining chlorine being essentially in the form of Cl (Schilke, Phillips & Wang 1995; Neufeld & Wolfire 2009).

In the dense ISM, HCl was first identified by Blake et al. (1985) in the OMC-1 and the HCl emission in OMC-1 was later reobserved and mapped by Schilke et al. (1995). Schilke et al. (1995) have shown, in particular, that HCl emission can be used as a tracer of very dense regions ($>10^7$ cm^{-3}). HCl was also observed in other molecular clouds such as Sagittarius B2 (Zmuidzinas et al. 1995). More recently, HCl emission of the two isotopologues, $H^{35}Cl$ and $H^{37}Cl$, was observed using HIFI-*Herschel* observations towards the carbon-rich star IRC+10216 (Cernicharo et al. 2010b; Agúndez et al. 2011), where lines from $j = 1-0$ up to $j = 7-6$ were detected, towards the protostellar shock L1157-B1 (Codella et al. 2012) and the star-forming region W3A (Cernicharo et al. 2010a). These new observations have provided new insight into the chlorine chemistry in dense and warm ($T > 150$ K) regions.

Thus, in the envelope of the star IRC+10216 where HCl is the major molecular reservoir of chlorine, the HCl abundance was found to be 1.1×10^{-7} relative to H_2. Once taken into account the abundance of the other chlorine-bearing species, it gives an abundance of 8×10^{-8} for the chlorine in molecular species, relative to H. This corresponds only to one quarter of the Cl solar abundance (3.2×10^{-7}), indicating a depletion of Cl on to dust grains and/or some chlorine in the form of gaseous atomic Cl (Agúndez et al. 2011). In L1157-B1, the HCl abundance was found to be even smaller, i.e. $3-6\times 10^{-9}$ relative to H_2 (Codella et al. 2012). While this abundance is similar to that observed towards low- and high-mass protostars, it actually suggests that HCl is a negligible reservoir of chlorine in both the gas and icy phase of star-forming regions. Indeed, the shock in L1157-B1 is strong enough to release molecules from the grains, and chlorine must be therefore in species other than HCl. On the other hand, HCl infrared absorption lines have been detected in the warm circumstellar environment of the protostar CRL 2136, with a fractional abundance of $1-2\times 10^{-7}$ relative to H_2 (Goto et al. 2013). This value corresponds to approximately 20 per cent of the elemental chlorine abundance, as predicted by the models of dense molecular clouds.

The estimation of HCl abundance from emission spectral lines requires the use of collisional rate coefficients with H_2, the most abundant interstellar species. Without these rates, only approximate estimates of the molecular abundances are possible assuming local thermodynamic equilibrium (LTE), which is generally not a good approximation at typical interstellar densities. Rate coefficients for the rotational/hyperfine excitation of HCl by He atoms (employed as substitute for H_2) have been calculated by Neufeld & Green (1994, hereafter NG) several years ago and revisited recently by Lanza & Lique (2012). Yang & Stancil (2014) also computed HCl–He rate coefficients for a large range of temperatures but neglected the hyperfine structure. Their rate coefficients at low temperatures were in very good agreement with those of Lanza & Lique (2012). He and H_2 rate coefficients can significantly differ in particular for molecular hydrides (Guillon & Stoecklin 2012), and it seems crucial to determine the actual HCl–H_2 rate coefficients.

In this paper, we provide the first set of collisional data for the HCl–H_2 system. A detailed comparison with the available set of data of NG and Lanza & Lique (2012) for HCl–He is also presented (both sets are scaled by 1.38). As a first astrophysical application and in order to illustrate the influence of our new rate coefficients on astrophysical models, we also perform radiative transfer calculations to simulate the excitation of HCl in star-forming regions and protostellar shocks. We also provide HCl–e^- rate coefficients, using the Born approximation, since the electron fraction in protostellar shocks can be high ($\gtrsim 10^{-5}$) and electron-impact excitation can play a role.

This paper is organized as follows: Section 2 describes briefly the ab initio calculations of the potential energy surface (PES) and of the dynamical computations. The results are presented and discussed in Section 3. In Section 4, we present a first astrophysical application of the present rate coefficients. Conclusions are given in Section 5.

2 THEORETICAL APPROACH

2.1 Potential energy surface

Calculations of the HCl($X^1\Sigma^+$)–H_2 PES is described in detail in our previous paper (Lanza et al. 2014, hereafter Paper I). We only present here a short description of the PES.

Ab initio calculations of the PES of HCl–H_2 van der Waals complex were carried out at the coupled cluster with single, double and perturbative triple excitation [CCSD(T)] (Hampel, Peterson & Werner 1992; Watts, Gauss & Bartlett 1993) level of theory using the MOLPRO 2010 package (Werner et al. 2010). The calculations were performed in the rather large augmented correlation-consistent quadruple zeta (aug-cc-pVQZ) basis set (Dunning 1989) augmented with bond functions defined by Williams et al. (1995).

Then, in order to solve the close-coupling equations for scattering, the PES was expanded over angular functions using the expression of Green (1975). The angular functions are formed from coupled spherical functions $Y_{l_i m_i}(\alpha, \beta)$ which are associated with the rotational angular momenta of HCl and H_2.

The global minimum of the 4D PES corresponds to the T-shape structure with the H_2 molecule on the H side of the HCl molecule with a well depth of $\Delta E = -213.38$ cm^{-1}. A secondary minimum corresponds also to a T-shape geometry but for the H_2 molecule on the Cl side with $\Delta E = -99.09$ cm^{-1}. We have found that the anisotropy of the PES, with respect to the HCl plane of rotation, is qualitatively similar to HCl–He anisotropy (Lanza & Lique 2012). However, the well depth is significantly larger in the case of interaction with H_2. A relatively strong anisotropy of the PES with respect to the H_2 rotation is also found. The experimental dissociation energy of the HCl–ortho-H_2 ($D_0 = 45 \pm 2$ cm^{-1}; Anderson, Schuder & Nesbitt 1998) was well reproduced by the calculated value from

our PES ($D_0 = 42.3$ cm^{-1}). Such agreement shows the accuracy of our PES calculation.

2.2 Scattering calculations

In this paper, j_1 and j_2 designate the rotational levels of HCl and H_2 respectively, such as

$$\mathrm{HCl}(j_1) + \mathrm{H_2}(j_2) \rightarrow \mathrm{HCl}(j_1') + \mathrm{H_2}(j_2).$$

We only consider the transitions where j_2 remains fixed, and equal to 0 or 2, corresponding to the two lowest rotational state for para-H_2 and equal to 1 for the lowest one of ortho-H_2. (De-)excitation of the H_2 during the collisions has been taken into account in the scattering calculations but we do not show the results since they are 2–3 orders of magnitude smaller than H_2 rotational state conserving transitions (Paper I). The calculations were performed for $H^{35}Cl$, but the results can be also used with confidence for $H^{37}Cl$ (less than 1 per cent of reduced mass difference). Although Cl has a non-zero nuclear spin ($I = 3/2$), we have neglected in the scattering calculations the hyperfine structure of the molecule. Results including the hyperfine structure will be presented elsewhere since HCl hyperfine resolved rate coefficients can be crucial in detailed models of radiative transfer (Daniel, Cernicharo & Dubernet 2006; Cernicharo et al. 2010a).

Recent scattering calculations have been published in Paper I. We refer the reader to Paper I for scattering calculation details. In summary, scattering calculations were performed with the MOLSCAT program (Hutson & Green 1994) using the close coupling approach (Green 1975). Calculations were carried out for total energies ranging from 0.5 to 3000 cm^{-1} for collisions of HCl with para-H_2 and ortho-H_2. We considered transitions between the first 11 ($j_1 = 0$–10) rotational states of HCl. In all the calculations, the H_2 rotational basis included $j_2 = 0$–2 and $j_2 = 1$–3 for para-H_2 and ortho-H_2, respectively. The convergence of the cross-sections with respect to the HCl and H_2 rotational basis has been discussed in details in Paper I. We found that the present rate coefficients are converged at better than 5 per cent for transitions involving $j_2 = 0$ and at better than 5–10 per cent for transitions involving $j_2 = 2$ (with respect to the PES used).

From the calculated cross-sections, one can obtain the corresponding thermal rate coefficients at temperature T by an average over the collision energy (E_c):

$$k_{j_1,j_2\rightarrow j_1',j_2}(T) = \left(\frac{8}{\pi\mu k_B^3 T^3}\right)^{1/2} \times \int_0^\infty \sigma_{j_1,j_2\rightarrow j_1',j_2}\, E_c\, \mathrm{e}^{-\frac{E_c}{k_B T}}\, \mathrm{d}E_c, \quad (1)$$

where $\sigma_{j_1,j_2\rightarrow j_1',j_2}$ is the cross-section, μ is the reduced mass of the system and k_B is the Boltzmann constant. Calculations up to 3000 cm^{-1} allow determining rate coefficients from 5 to 300 K.

3 RESULTS AND DISCUSSION

3.1 Rotational transitions

We have obtained the rotational rate coefficients of HCl in collision with both para-H_2 and ortho-H_2. The complete set of (de-)excitation rate coefficients is available online from the LAMDA (Schöier et al. 2005) and BASECOL (Dubernet et al. 2013) websites.

The variation with temperature of typical HCl–H_2 de-excitation rate coefficients is presented in Fig. 1 for both para-H_2 and ortho-H_2.

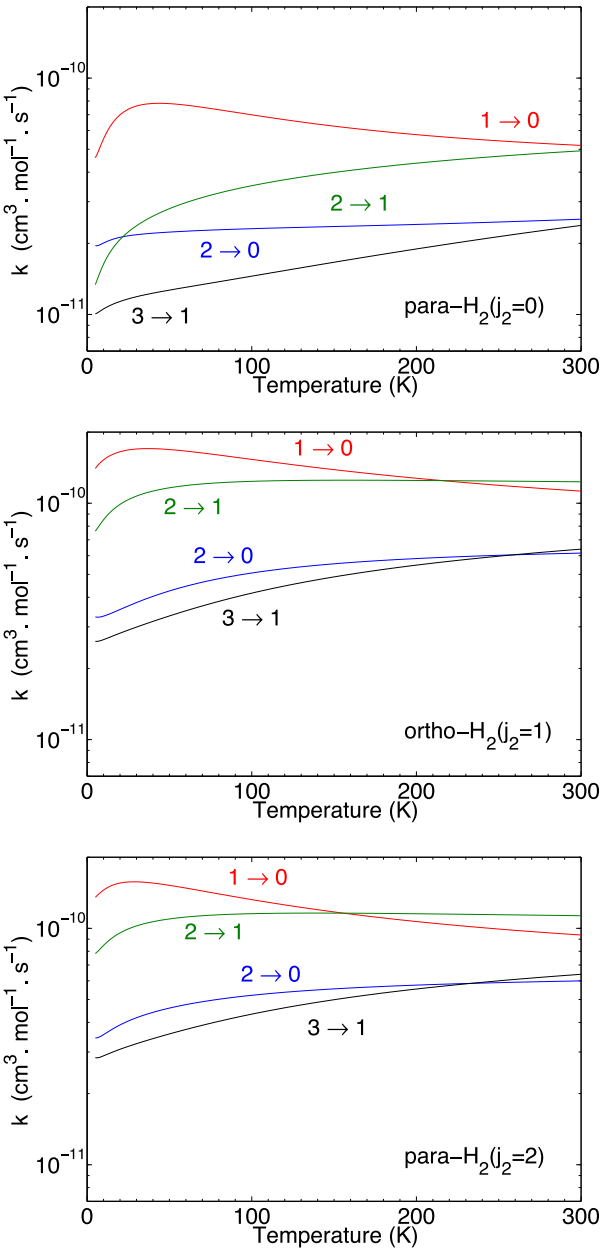

Figure 1. Typical rotational de-excitation rate coefficients of HCl by para-H_2($j_2 = 0$) (upper panel), ortho-H_2($j_2 = 1$) (middle panel) and para-H_2($j_2 = 2$) (lower panel). From initial level j_1 to final level j_1'.

First of all, we can notice that the rate coefficients vary smoothly with the temperature especially above 50 K. Then, we can observe that for a given HCl rotational transition, the rate coefficients are generally two to three times smaller for collisions with para-H_2(j_2=0) than for collisions with H_2($j_2 > 1$). Such effect can be more clearly seen in Fig. 2 that shows the three first $\Delta j_1 = 1$ de-excitation transitions, for both para-H_2($j_2 = 0$) and ortho-H_2($j_2 = 1$). Even if ortho-H_2 is significantly less abundant than para-H_2($j_2 = 0$) in the cold ISM, the magnitude of the ortho-H_2 rate coefficients make that this collisional partner has to be included as soon as the ortho-to-para ratio (OPR) of H_2 is over 1/10. One can also notice in Fig. 1 that rate coefficients for collisions with para-H_2($j_2 = 2$) and ortho-H_2($j_2 = 1$) are very similar (see Paper I). Then, in the following, we do not discuss anymore the para-H_2($j_2 = 2$) results

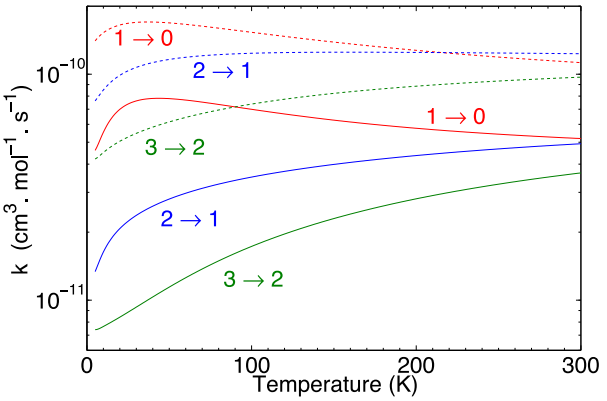

Figure 2. $\Delta j_1 = 1$ rotational de-excitation rate coefficients of HCl by para-$H_2(j_2 = 0)$ (solid lines) and ortho-$H_2(j_2 = 1)$ (dashed lines). From initial level j_1 to final level j_1'.

and consider that discussion about ortho-$H_2(j_2 = 1)$ data also apply for them.

An interesting feature of the HCl–H_2 rate coefficients is that the rate coefficients for the $j_1 = 1 \rightarrow j_1' = 0$ transition is about two times larger than the $j_1 = 2 \rightarrow j_1' = 1$ transition. This is a noticeable difference with other diatomic species in collision with H_2 like CO (Wernli et al. 2006) or SiS (Kłos & Lique 2008) where the opposite behaviour is observed. Such effect is also observed in HF–H_2 (Guillon & Stoecklin 2012) or in HCl–He (Lanza & Lique 2012) rate coefficients. This behaviour may be specific to hydrides for which the energy spacing between consecutive rotational states significantly increase with increasing rotational state.

Fig. 3 displays all the de-excitation transitions starting from $j_1 = 5$ for three temperatures and for both para-H_2 and ortho-H_2. Such a figure allows us to see the Δj_1 influence on the intensities of the rate coefficients.

We can observe that the rate coefficients decrease while Δj_1 increase for both para- and ortho-H_2. We can retrieve the predominance of the $\Delta j_1 = 1$ transitions over the $\Delta j_1 = 2$ ones already found in Paper I. There is also, in the case of para-$H_2(j_2 = 0)$, a predominance of the $\Delta j_1 = 3$ transitions over the $\Delta j_1 = 4$ ones, which confirms the propensity rules in favour of odd Δj_1 transitions for collisions with para-$H_2(j_2 = 0)$.

However, for para-H_2, the propensity rule in favour of odd transitions is more effective at low temperature, as it can be clearly observed in Fig. 3 at temperature of 10 and 100 K, where transitions with $\Delta j_1 = 3$ give higher rate coefficients than the ones with $\Delta j_1 = 2$.

For ortho-$H_2(j_2 = 1)$, the propensity rule weakens, leading to the observation of a bump at low temperature (10 K) and tending to an exponential gap law with increasing temperature. Such a propensity rule in favour of odd transitions, even if not too marked in this case, is a classical trend for heteronuclear molecules, such as HCl, which have an odd anisotropic PES, as discussed in detail in Paper I.

Finally, we compared the HCl–H_2 rate coefficients with those of another similar halogen hydride, the HF hydride (Guillon & Stoecklin 2012). We found that the magnitude of the rate coefficients for transitions with $\Delta j_1 = 1$ are of the same order of magnitude for both molecules. On the other hand, transitions with $\Delta j_1 = 2$ are much smaller in the case of HF than in the case of HCl (one or two orders of magnitude). Two effects significantly contribute to these differences: (i) the odd anisotropy of the HF–H_2 PES is much larger than the one of the HCl–H_2 PES leading to a stronger propensity

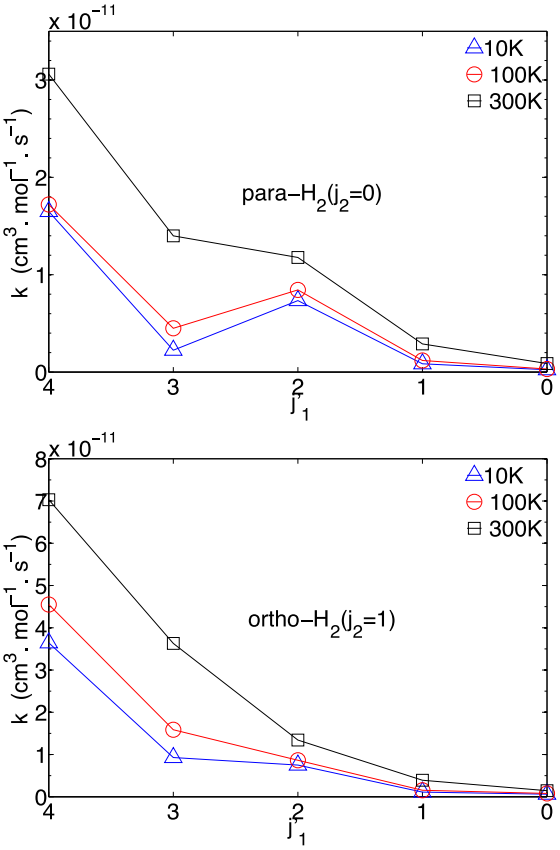

Figure 3. Propensity rules for transitions out of the initial $j_1 = 5$ state of the HCl molecule in collision with H_2, for temperature=10, 100 and 300 K: para-$H_2(j_2 = 0)$ (upper panel) and ortho-$H_2(j_2 = 1)$ (lower panel).

in favour of $\Delta j_1 = 1$ and (ii) the larger energy spacing between HF rotational states make the rotational energy transfers $\Delta j_1 > 1$ less efficient.

3.2 Comparison between H_2 and He rate coefficients

Until now, the HCl rate coefficients available in astrophysical data base were those of NG and more recently those of Lanza & Lique (2012) computed with He as collisional partner. In order to model HCl–H_2 rate coefficients, astronomers usually apply a scaling factor of 1.38 (Schöier et al. 2005) on the HCl–He rate coefficients. This scaling factor comes from the assumption that the velocity-averaged cross-sections of HCl–He and HCl–para-$H_2(j_2=0)$ are equal. In that case, the difference in the He and H_2 rate coefficients appears only because of the difference of the reduced mass μ of the two collisional systems, as can be observed in equation (1).

Then, we have compared our new rate coefficients to the previous He ones scaled by a factor of 1.38. The results are shown in Fig. 4 for four selected de-excitation transitions.

As already shown by Lanza & Lique (2012), one can observe that the two sets of HCl–He rate coefficients exhibit differences, particularly for $j_1 = 2 \rightarrow j_1' = 0$ transition. However, global agreement exists between the two sets of data. At the opposite, significant differences exist between H_2 and He $\times$ 1.38 rate coefficients. Differences can be greater than one order of magnitude, especially at low temperatures. The differences depend on the transitions and on the temperature but in general, He rate coefficients are much smaller than the H_2 ones, especially for ortho-H_2. Such differences lead to

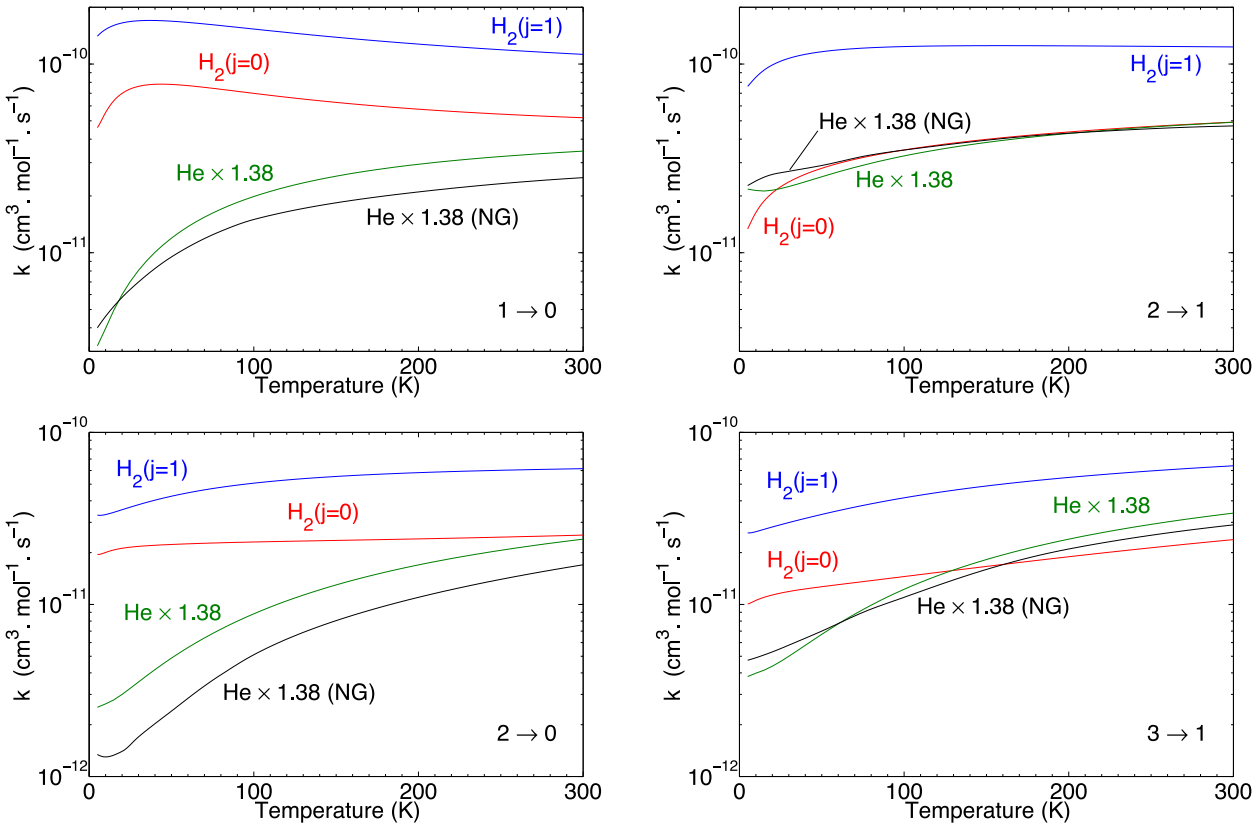

Figure 4. Rotational de-excitation rate coefficients of HCl by para-H_2($j_2 = 0$) (red lines), by ortho-H_2($j_2 = 1$) (blue lines) and by He scaled by 1.38 (Lanza & Lique 2012 : green lines and NG: black lines).

a conclusion that it is unrealistic to estimate H_2 rate coefficients by simply applying a scaling factor to the He rate coefficients. As a result, for HCl, as for other hydrides or small molecules like CO, estimation of the H_2 rate coefficients from the He ones appears to be an unsuccessful approximation (see e.g. Roueff & Lique 2013, and references therein). However, we note that for much heavier collisional systems, such as SiS–H_2 (Lique et al. 2008), HC_3N (Wernli et al. 2007) or CS (Lique, Spielfiedel & Cernicharo 2006; Denis-Alpizar et al. 2013), this approximation has been found to be accurate within a factor of 2. To summarize, even if this approximation can sometimes work, it is not recommended to use He rates in order to model H_2, as recently discussed by Walker et al. (2014).

In the light of these differences, we can expect that our rate coefficients for both para-H_2 and ortho-H_2 will have a significant influence on the modelling of the abundance of HCl in the ISM, and in particular in molecular clouds.

3.3 Interstellar HCl

As a first application and in order to test the impact of the HCl–H_2 rate coefficients, we have performed radiative transfer calculations for typical physical conditions from where HCl emission is observed. Non-LTE calculations were performed with the RADEX code (van der Tak et al. 2007) using the large velocity gradient approximation. Both collisional and radiative processes are taken into account, while optical depth effects are treated with an escape probability method. We also include the cosmic microwave background radiation at 2.73 K. In all the calculations, we consider a typical column density of $1{\sim}10^{13}$ cm^{-2}, a typical line width of 3.0 km s^{-1} and we assume a uniform spherical geometry of the cloud.

We have chosen parameters corresponding to typical physical conditions in star-forming regions and protostellar shocks. Indeed, interstellar HCl emission has been mainly observed in these environments (Schilke et al. 1995; Codella et al. 2012). We have simulated the excitation of HCl using the He rate coefficients of NG scaled by 1.38, our previously published He rate coefficients also scaled by 1.38 (Lanza & Lique 2012), and the present H_2 rate coefficients. It should be noted that the mass scaling approach is expected to be more accurate to model ground state para-H_2(j_2=0) than rotationally excited H_2 ($j_2 \geq 1$). However, this approximation is generally used to model both para- and ortho-H_2, without distinction. For the two temperatures (50 and 200 K) explored in this work, we have chosen for the OPR of H_2, the value of 0 (only para-H_2), the values corresponding to the thermal distribution of the two nuclear spin isomers (0.3 at 50K and 1 at 200 K) and the value of 3 corresponding to the high temperature limit. We note that the state-to-state rate coefficients for para-H_2 were averaged over a thermal (Boltzmann) rotational state distribution. Furthermore, in protostellar shocks, the electron abundance can be significant (up to 10^{-4} relative to H_2; Roberts et al. 2012) so that we also performed a set of calculations taking into account the highest abundance of electrons that can be found in these regions. Calculations of electron rate coefficients using the Born approximation are described in Appendix A of this paper.

Fig. 5 shows the simulated brightness temperature of the first two radiative transitions of HCl obtained at 50 K for typical physical conditions of star-forming regions. We can observe that the two sets of He rate coefficients lead to similar brightness temperatures despite the latest He rate coefficients slightly increasing the predicted line intensities.

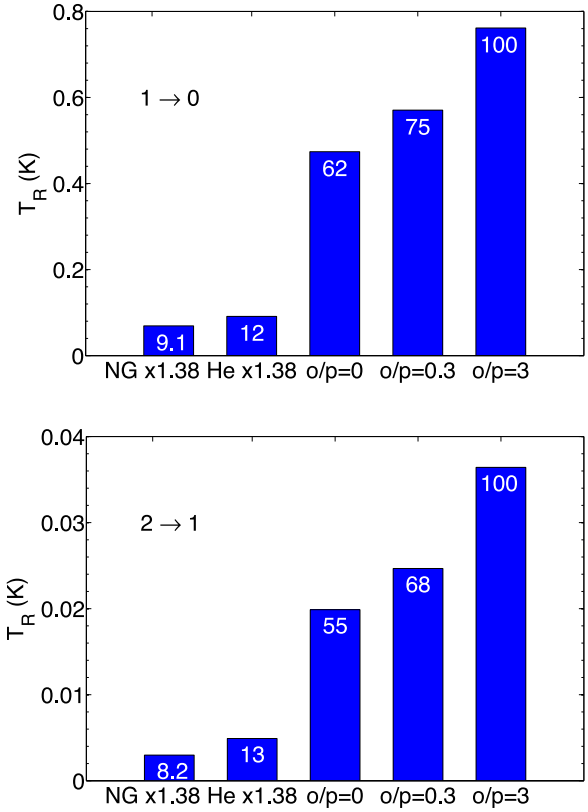

Figure 5. Brightness temperature (in K) of the first two radiative transitions of HCl for a kinetic temperature of 50 K and for density of the collision partner: $1{\sim}10^6$ cm^{-3}. Different sets of rate coefficients are shown from the left to the right: NG scaled by 1.38, He scaled by 1.38, para-H_2, H_2 with a ratio ortho/para=0.3 and 3 (the numbers on the histograms are percentages relative to the intensity of H_2 with a ratio ortho/para=3).

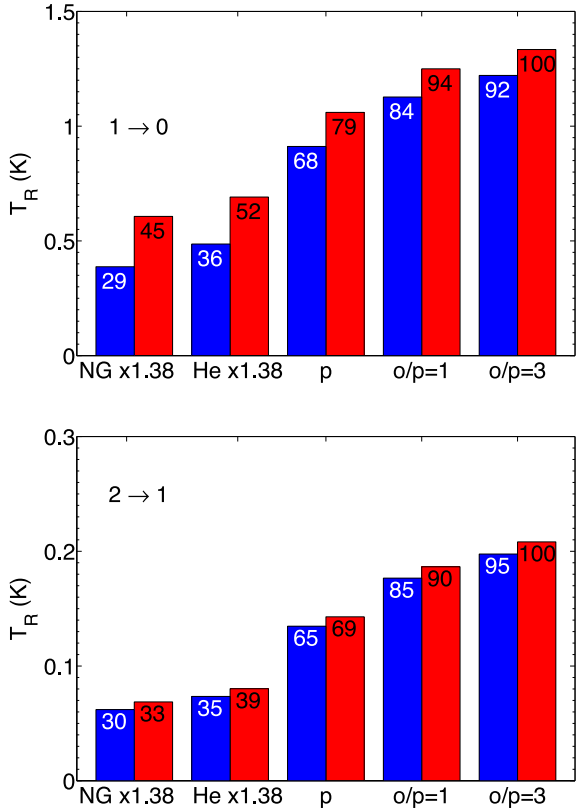

Figure 6. Brightness temperature (in K) of the first two radiative transitions of HCl for a kinetic temperature of 200 K and for density of the collision partner: $1{\sim}10^6$ cm^{-3}, without electrons (in blue) and with electrons, density: $1{\sim}10^2$ cm^{-3} (in red). Different sets of rate coefficients are shown from the left to the right: NG scaled by 1.38, He scaled by 1.38, para-H_2, H_2 with a ratio ortho/para=1 and 3 (the numbers on the histograms are percentages relative to the intensity of H_2 with a ratio ortho/para=3 and electrons).

The main impact is seen when replacing He rate coefficients by present H_2 rate coefficients. Indeed, the brightness temperatures significantly increase whatever the transitions are. The ratio between H_2 and He line intensities is of the factor 5–10 depending on the OPR of H_2. Such an increase is due to the large difference between scaled He and H_2 rate coefficients. HCl–H_2 rate coefficients are up to an order of magnitude larger than those of He. This increase is directly seen in the brightness temperature as we are in the optically thin regime. We also note that the OPR of H_2 in molecular clouds impacts the simulated line intensities. Indeed, results obtained taking into account only collisions with para-H_2 are up to a factor of 2 smaller than those obtained for a ortho–para-H_2 ratio of 3. Such difference can be simply explained by the largest magnitude of ortho-H_2 rate coefficients. It confirms the importance of having both para-H_2 and ortho-H_2 rate coefficients, as well as an estimate of the OPR of H_2, to perform an accurate modelling of HCl emission.

The present calculations show that HCl abundance derived from radiative transfer analysis performed using He rate coefficients (as it has been done presently) has been significantly overestimated. The overestimation can be larger than a factor of 5. It is then crucial to revise the HCl abundance in star-forming regions using the new collisional data.

Next, in order to model warmer interstellar regions, the same calculations have been performed at 200 K for the typical physical conditions of protostellar shocks. As mentioned above, we have performed calculations with and without taking into account electron collisions. The calculated brightness temperatures are displayed in Fig. 6.

The effects seen at 50 K are confirmed at 200 K. The He rate coefficients lead to smaller line intensities than the H_2 ones. The ratio being slightly smaller (2–3) at 200 K than at 50 K. Indeed, differences between He and H_2 rate coefficients decrease with increasing temperatures so that the effect of using He rate coefficients instead of H_2 leads to less inaccuracies than at low temperatures. Nevertheless, we also found that HCl abundance in protostellar shocks determined using He rate coefficients has been overestimated by at least a factor of 2–3.

We can also observe that adding electron collisions, with an electron fraction equal to 10^{-4}, leads to an increase in the brightness temperatures. The effect is most important for the $1 \rightarrow 0$ transition than for the other transition where the inclusion of electron collisions increases the intensities by about 5 per cent. The effect is more pronounced when using He rate coefficients than when using H_2 ones. Nevertheless, we can see that the effect of electron collisions is moderate even at high ionization fraction. This actually reflects the moderate value of the HCl dipole (1.1 D), see Appendix A.

Such comparisons show that it is crucial, for interpreting HCl emission observations, to take into account actual H_2 rate coefficients. They also show that the use of He rate coefficients leads to a significant overestimation of the HCl abundance in the dense ISM, the overestimation being more pronounced in cold than in warm

regions. As a result, HCl abundance derived from observations of protostellar shocks or star-forming regions has to be urgently revised.

4 CONCLUSIONS

We have computed the first set of rotational rate coefficients for the HCl–H_2 collisional system. We have found that previous scaled HCl–He and present HCl–H_2 rate coefficients differ significantly. Hence, HCl–He rate coefficients are not recommended for modelling HCl emission from molecular clouds. This is even more true when ortho-H_2 is in significant abundance in the ISM, since ortho-H_2 rate coefficients are two to three times larger than para-H_2 ones.

In order to evaluate the effect of these new data on the astrophysical modelling, we have performed radiative transfer calculations corresponding to typical physical conditions of the ISM where HCl emission is detected. The simulated brightness temperatures obtained with our new rate coefficients are significantly larger than the ones obtained with previous He rate coefficients. At 50 K, the new rates lead to an increase by a factor of 5–10 of the brightness temperatures, depending on the OPR of H_2. At 200 K, the effect is slightly less important but brightness temperature increases by a factor of 2–3 also depending on the OPR of H_2.

With these new results, the HCl abundance derived from the observations will be substantially smaller than the current estimates. In particular, for the shock in L1157-B1, we can predict an HCl abundance of $1-3 \times 10^{-9}$ relative to H_2 (i.e. a factor of 2–3 smaller than Codella et al. 2012), thus confirming that HCl is a negligible reservoir of chlorine in this source. More generally, it means that, in the dense ISM, chlorine is probably in other species than HCl and that HCl is much less abundant than previously supposed. At the opposite of HF that is directly formed through the F+H_2 reaction (Tizniti et al. 2014), the facts that Cl does not react efficiently with H_2 and that HCl molecule is formed through multiple gas-phase reactions probably lead to many uncertainties on the HCl formation pathways. In addition, the fact that HCl can be destroyed by H collisions (even if it is slow) also raises many questions regarding the HCl chemistry that needs to be better understood through laboratory or theoretical studies using state-of-the-art methods. The recent HIFI-*Herschel* detection of chlorine-bearing ions, HCl^+ and H_2Cl^+, will also certainly help in resolving the puzzle of the chlorine chemistry and in determining the abundance of each chlorine-bearing species.

ACKNOWLEDGEMENTS

This research was supported by the Agence Nationale de la Recherche (ANR-HYDRIDES), contract ANR-12-BS05-0011-01. Support by the CNRS national programme 'Physique et Chimie du Milieu Interstellaire' is also acknowledged. We also thank the CPER Haute-Normandie/CNRT/Energie, Electronique, Matériaux.

REFERENCES

Agúndez M., Cernicharo J., Waters L. B. F. M., Decin L., Encrenaz P., Neufeld D., Teyssier D., Daniel F., 2011, A&A, 533, L6
Anderson D. T., Schuder M., Nesbitt D. J., 1998, Chem. Phys., 239, 253
Asplund M., Grevesse N., Sauval A. J., Scott P., 2009, ARA&A, 47, 481
Blake G. A., Keene J., Phillips T. G., 1985, ApJ, 295, 501
Cernicharo J., Guelin M., 1987, A&A, 183, L10
Cernicharo J. et al., 2010a, A&A, 518, L115
Cernicharo J. et al., 2010b, A&A, 518, L136
Codella C. et al., 2012, ApJ, 744, 164
Daniel F., Cernicharo J., Dubernet M.-L., 2006, ApJ, 648, 461
Denis-Alpizar O., Stoecklin T., Halvick P., Dubernet M.-L., 2013, J. Chem. Phys., 139, 204304
Dubernet M.-L. et al., 2013, A&A, 553, A50
Dunning T. H., 1989, J. Chem. Phys., 90, 1007
Federman S. R., Cardell J. A., van Dishoeck E. F., Lambert D. L., Black J. H., 1995, ApJ, 445, 325
Goto M., Usuda T., Geballe T. R., Menten K. M., Indriolo N., Neufeld D. A., 2013, A&A, 558, L5
Green S., 1975, J. Chem. Phys., 62, 2271
Guillon G., Stoecklin T., 2012, MNRAS, 420, 579
Hampel C., Peterson K. A., Werner H.-J., 1992, Chem. Phys. Lett., 190, 1
Hutson J. M., Green S., 1994. MOLSCAT computer code, version 14, distributed by Collaborative Computational Project No. 6 of the Engineering and Physical Sciences Research Council (UK)
Itikawa Y., Mason N., 2005, Phys. Rep., 414, 1
Kłos J., Lique F., 2008, MNRAS, 390, 239
Lanza M., Lique F., 2012, MNRAS, 424, 1261
Lanza M., Kalugina Y., Wiesenfeld L., Lique F., 2014, J. Chem. Phys., 140, 064316 (Paper I)
Lide D. R., 2008, CRC Handbook of Chemistry and Physics: a Ready-Reference Book of Chemical and Physical Data. CRC Press, Boca Raton, FL
Lique F., Spielfiedel A., Cernicharo J., 2006, A&A, 451, 1125
Lique F., Toboła R., Kłos J., Feautrier N., Spielfiedel A., Vincent L. F. M., Chałasiski G., Alexander M. H., 2008, A&A, 478, 567
Lis D. C. et al., 2010, A&A, 521, L9
Luca M. D. et al., 2012, ApJ, 751, L37
Monje R. R., Lis D. C., Roueff E., Gerin M., De Luca M., Neufeld D. A., Godard B., Phillips T. G., 2013, ApJ, 767, 81
Neufeld D. A., Green S., 1994, ApJ, 432, 158 (NG)
Neufeld D. A., Wolfire M. G., 2009, ApJ, 706, 1594
Neufeld D. A. et al., 2012, ApJ, 748, 37
Novotný O. et al., 2012, J. Phys. Conf. Ser., 388, 062047
Novotný O. et al., 2013, ApJ, 777, 54
Pfingst K., Thummel H. T., Peyerimhoff S. D., 1992, J. Phys. B. At. Mol. Opt. Phys., 25, 2107
Roberts J. F., Jiménez-Serra I., Gusdorf A., Martín-Pintado J., 2012, A&A, 544, A150
Roueff E., Lique F., 2013, Chem. Rev., 113, 8906
Schilke P., Phillips T. G., Wang N., 1995, ApJ, 441, 334
Schöier F. L., van der Tak F. F. S., van Dishoeck E. F., Black J. H., 2005, A&A, 432, 369
Smith D., Adams N. G., 1981, MNRAS, 197, 377
Tizniti M., Le Picard S. D., Lique F., Berteloite C., Canosa A., Alexander M. H., Sims I. R., 2014, Nat. Chem., 6, 141
van der Tak F., Black J., Schoeier F., Jansen D., van Dishoeck E., 2007, A&A, 468, 627
Wakelam V. et al., 2012, ApJS, 199, 21
Walker K. M., Yang B. H., Stancil P. C., Balakrishnan N., Forrey R. C., 2014, ApJ, 790, 96
Watts J. D., Gauss J., Bartlett R. J., 1993, J. Chem. Phys., 98, 8718
Werner H.-J. et al., 2010, MOLPRO, version 2010.1, a package of ab initio program, available at: http://www.molpro.net
Wernli M., Valiron P., Faure A., Wiesenfeld L., Jankowski P., Szalewicz K., 2006, A&A, 446, 367
Wernli M., Wiesenfeld L., Faure A., Valiron P., 2007, A&A, 475, 391
Williams H. L., Mass E. M., Szalewicz K., Jeziorski B., 1995, J. Chem. Phys., 103, 7374
Yang B., Stancil P. C., 2014, ApJ, 783, 92
Zmuidzinas J., Blake G. A., Carlstrom J., Keene J., Miller D., 1995, ApJ, 447, L125

APPENDIX A: HCL–e^- RATE COEFFICIENTS

A number of experimental and theoretical results are available for the electron-impact rotational excitation of HCl (see Itikawa

& Mason 2005 and references therein). In particular, Pfingst, Thummel & Peyerimhoff (1992) carried out rotational close-coupling calculations by combining the **R**-matrix method with the adiabatic-nuclei-rotation approximation and applying the frame transformation at the **R**-matrix boundary. Pfingst et al. (1992) were thus able to obtain rotational cross-sections with the proper threshold behaviour, in contrast to the usual asymptotic frame transformation procedure. Their results were shown to be in good agreement with differential data measured above 0.5 eV. In the case of dipolar transitions ($\Delta j_1 = 1$), their results were also found to be in good agreement with Born cross-sections, down to collision energies of a few meV. In the case of polar molecules, the long-range electronic dipole interaction is well known to dominate the rotational excitation, especially at low collision energies. The HCl dipole is moderate, 1.1 D, but dipolar transitions dominate in HCl. Thus, at low energy (<1 eV), the $j_1 = 0 \rightarrow j_1' = 2$ cross-section is typically two orders of magnitude smaller than the $j_1 = 0 \rightarrow j_1' = 1$ transition (Itikawa & Mason 2005).

We have computed the rotational cross-sections for HCl–e$^-$ by using the dipolar Born approximation. The explicit formula can be found e.g. in equation 39 of Itikawa & Mason (2005). Only transitions with $\Delta j_1 = 1$ were thus considered. The HCl dipole was taken as 1.1 D. The first 11 levels ($j_1 = 0-10$) of HCl were included and the corresponding cross-sections were computed for energies ranging from 2 meV to 1 eV. Rate coefficients were deduced for temperatures from 10 to 1000 K. For de-excitation transitions ($\Delta j_1 = -1$), the rate coefficients lie in the range 1–5 $\times$ 10^{-7} cm^3 s^{-1}, i.e. typically 3–4 orders of magnitude larger than the H_2 rate coefficients, and they should be accurate to within a factor of 2. The complete set of de-excitation rate coefficients is available online from the LAMDA (Schöier et al. 2005) and BASECOL (Dubernet et al. 2013) data base.

This paper has been typeset from a TEX/LATEX file prepared by the author.